JOURNAL OF SOLID STATE CHEMISTRY 44, 89–98 (1982)

$CaMnO_{2.5}$ and $Ca_2MnO_{3.5}$: New Oxygen-Defect Perovskite-Type Oxides*

K. R. POEPPELMEIER,† M. E. LEONOWICZ, AND J. M. LONGO

Exxon Research and Engineering Company, P.O. Box 45, Linden, New Jersey 07036

Received November 2, 1981

We found that when the precursors $CaMnO_3$ and Ca_2MnO_4 are reduced with any one of a variety of inorganic (H_2, NH_3) or organic (C_2H_4, C_3H_6) reducing agents between 300 and 500°C, topotactic reaction occurs to produce the ordered oxygen-defect phases $CaMnO_{2.5}$ and $Ca_2MnO_{3.5}$, respectively. Orthorhombic cell constants for $CaMnO_{2.5}$ are $a = 5.43(1)$, $b = 10.24(1)$, and $c = 3.74(1)$ Å, and for $Ca_2MnO_{3.5}$ are $a = 5.30(1)$, $b = 10.05(1)$, and $c = 12.24(1)$ Å. These compounds were characterized by powder X-ray diffraction, thermogravimetric analysis, magnetic susceptibility, and infrared spectroscopy. The reduced compounds reversibly oxidize to their respective precursor in oxygen at low temperatures.

Introduction

The synthesis of nonstoichiometric compounds often depends on the structure of the starting material since this feature can have a large influence on a material's reactivity. Examples include intercalation compounds of graphite and other layered compounds, layer silicates and their cation exchange capabilities, and the oxide shear phases of Group VB and VIB transition metals. Syntheses of the kind that depend on existing structural elements in the starting material often result in metastable compounds, and are usually carried out at relatively low temperatures. Anion-deficient ABO_{3-x} perovskites (*1*), in contrast, are generally prepared by reduction at temperatures greater than 1000°C, where equilibrium with respect to oxygen is attained rapidly. Thus, compounds that are metastable or stable only at lower temperatures are lost. In this paper the low-temperature preparations of the perovskite-related compounds $CaMnO_{2.5}$ and $Ca_2MnO_{3.5}$ are described. Their structures were determined from powder X-ray diffraction data. The results reveal an ordering of the oxygen vacancies not seen before in perovskite-related structures and an unusual square pyramidal coordination ($\sim C_{4v}$) for the Mn^{3+} cations. Our results lead us to speculate that some, if not all, composition limits and associated structural transformations reported for the compounds $AMnO_{3-x}$, $A = Sr^{2+}$ or Ba^{2+}, result from ordered oxygen

* Dedicated to Professor A. F. Wells on his 70th birthday.

† To whom correspondence should be addressed.

0022-4596/82/100089-10$02.00/0

defects of the same type found in $CaMnO_{2.5}$ and $Ca_2MnO_{3.5}$.

Preparation

The starting materials $CaMnO_3$ and Ca_2MnO_4 used in this study were prepared in polycrystalline form from their calcite precursors $CaMn(CO_3)_2$ and $Ca_2Mn(CO_3)_3$ by oxidative decomposition at 1000°C in air as described by Horowitz and Longo (*2*). Unreacted carbonate precursor could not be detected in the powder X-ray diffraction patterns or infrared spectra of the products after calcination. The reduction of $CaMnO_3$ and Ca_2MnO_4 was studied from room temperature to 600°C with a variety of inorganic (H_2, NH_3) and organic (C_2H_4, C_3H_6) reducing agents supplied premixed by Matheson Gas Company. Typically, 3–5 g of sample was placed in an alumina boat and then jacketed in a 22 mm (i.d.) × 45 cm Vycor tube with an entrance port and exit bubbler. Next, the system (170 cm^3) was flushed at 50 cm^3/min for 30 min while at room temperature. The flow was adjusted to 10–15 cm^3/min while the tube was brought to the desired temperature in a conventional resistance-heated furnace. The temperature was monitored with a thermocouple attached to the outside of the Vycor jacket. In 10% H_2/He the reduction of $CaMnO_3$ or Ca_2MnO_4 to $CaMnO_{2.5}$ or $Ca_2MnO_{3.5}$ was possible only in the narrow temperature range 300–325°C in order to prevent the formation of the rock salt Mn^{2+} phases $CaMnO_2$ or Ca_2MnO_3, respectively (Eqs. (1) and (2)). As a result of the low temperatures used in the preparations long reaction times in excess of 100 hr were required to prepare $CaMnO_{2.5}$ or $Ca_2MnO_{3.5}$ from their oxidized precursors.

$$CaMnO_3(s) \xrightarrow[300°C]{H_2} CaMnO_{2.5}(s) \xrightarrow[325°C]{H_2} CaMnO_2(s) \quad (1)$$

$$Ca_2MnO_4(s) \xrightarrow[300°C]{H_2} Ca_2MnO_{3.5}(s) \xrightarrow[325°C]{H_2} Ca_2MnO_3(s) \quad (2)$$

Below 300°C little or no reduction was observed and above 325°C significant amounts of $CaMnO_2$ or Ca_2MnO_3 were formed. All characterization studies described in succeeding sections were on samples prepared by hydrogen reduction at or near 300°C. When other gas mixtures such as 5% NH_3, C_2H_4, or C_3H_6 in helium were substituted for dilute hydrogen in the preparation of $CaMnO_{2.5}$ or $Ca_2MnO_{3.5}$, reduction was found to occur over the temperature range 400–500°C and thus at a considerably faster rate. The carbon dioxide produced from the oxidation of ethylene or propylene leads to some formation of carbonates. By using ammonia, the formation of carbonate can be eliminated.

Single crystals of $CaMnO_3$ and Ca_2MnO_4 up to 0.5 mm maximum dimension were grown from $CaCl_2$ fluxes. $CaMnO_3$ was found to be orthorhombic with a = 5.279(1), b = 7.448(1), and c = 5.264(1) Å, as reported in the literature (*3*). While the tetragonal K_2NiF_4 structure reported for Ca_2MnO_4 (*4*) is qualitatively correct, the actual structure has a larger unit cell with a = 5.183 (1) and c = 24.117 (4) Å. Details of these studies will be published elsewhere. When the crystals were reduced by the methods described in the previous paragraph, they were transformed into an essentially polycrystalline state, even though their exterior physical appearance was unaltered. This negative result has necessitated characterization techniques using polycrystalline $CaMnO_{2.5}$ and $Ca_2MnO_{3.5}$ samples.

Characterization

The purity of the oxidized phases $CaMnO_3$ and Ca_2MnO_4, prepared from their calcite precursors, was verified with powder X-ray diffraction and the cell pa-

rameters reported in the literature (*3*, *4*). Cation stoichiometries were determined by reducing the oxides in hydrogen for 2 hr at 1000°C. The linear variation in the cubic unit cell parameter of the single phase, solid-solution $Ca_{1-x}Mn_x$ O, $0 \leq x \leq 1$, was used to determine the percentage of atomic calcium and manganese to within ±0.25% as reported. Oxygen content of the oxidized and reduced compositions was established by hydrogen reduction using a Fisher thermogravimetric analyzer equipped with a Cahn electrobalance. Weight loss was attributed to manganese with oxidation states greater than two. Their compositions determined by experiment were within 1 at.% of oxygen of the theoretical values of $CaMnO_{3.0}$, $CaMnO_{2.5}$, $Ca_2MnO_{4.0}$, and $Ca_2MnO_{3.5}$.

An important feature of the oxygen-deficient compounds is their ease of reoxidation with restoration of their initial composition and structure. Reoxidation is very rapid in air at temperatures as low as 300°C, and the cycle of reduction–reoxidation can be repeated any number of times without sample degradation. Figure 1 is a TGA trace of one reversible redox cycle of $CaMnO_{3-x}$ followed by irreversible reduction to $CaMnO_2$.

The symmetry and local coordination of

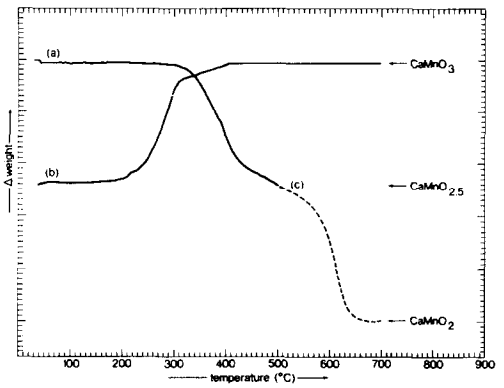

FIG. 1. Thermogravimetric analysis of $CaMnO_{3.0}$ in (a) 10% H_2/He to 500°C, (b) followed by air reoxidation, and then irreversible reduction (a + c).

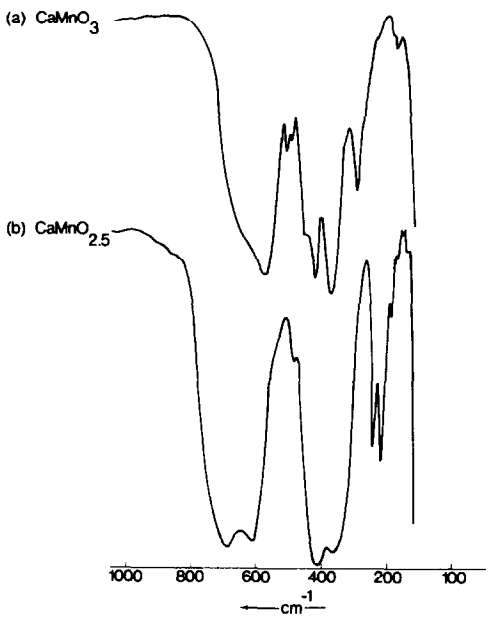

FIG. 2. Infrared spectra of $CaMnO_{3.0}$ (a) and $CaMnO_{2.5}$ (b).

the oxidized and reduced manganese sites in $CaMnO_{3-x}$ were studied with infrared spectroscopy. Spectra were recorded on a Digilab FTS-14A spectrometer using pressed KBr (4000–400 cm^{-1}) and CsI (500–100 cm^{-1}) pellets. The spectra are compared in Fig. 2.

The magnetic susceptibility of $CaMnO_{2.5}$ was measured in the range 77–600K using a Faraday apparatus. The high Neel temperature (T_N) of ~350K has made it difficult to obtain an accurate extrapolation of the high-temperature data. However, it is clear that $CaMnO_{2.5}$ contains high-spin Mn^{3+} above T_N with $5.65 \geq \mu_{obs} \geq 4.9$ and $-790 \leq \theta \leq -445$ ($\mu_{s.o.} = 4.9$ for Mn^{3+}).

Crystallographic Study

The phase purity, cell parameters, and structure of $CaMnO_{2.5}$ and $Ca_2MnO_{3.5}$ were determined from powder X-ray diffraction data recorded with a Philips diffractometer using Cu$K\alpha$ radiation and a graphite crystal

diffracted-beam monochromator. The spectra were recorded at a scan rate of 0.25°/min. Figure 3 compares the XRD pattern of $CaMnO_3$ with $CaMnO_{2.5}$ and shows the underlying intensity patterns characteristic of a cubic perovskite with a unit cell parameter of approximately 3.7 Å. The XRD patterns of $CaMnO_{2.5}$ and $Ca_2MnO_{3.5}$ were indexed on the basis of similar distortions of the 3.7-Å distance characteristic of the linear Mn–O–Mn array of the oxidized precursors. The structural relationship can be expressed by the equation $(a_o + b_o/2)/2 = a_c\, 2^{1/2}$. In this equation, a_o and b_o are the new orthorhombic unit cell parameters that are related by the equality shown to the pseudocubic quantity a_c. The unit cell for $CaMnO_{2.5}$ was determined to be orthorhombic with $a = 5.43(1)$, $b = 10.24(1)$, and $c = 3.74(1)$ Å, and for $Ca_2MnO_{3.5}$ to be again orthorhombic with $a = 5.30(1)$, $b = 10.05(1)$, and $c = 12.24(1)$ Å. High-resolution Guinier films obtained with monochromatized Cu $K\alpha_1$ radiation with an Enraf–Nonius Model FR-552 camera were consistent with the orthorhombic unit cells used to index the diffractometer data. Intensity data were measured for $CaMnO_{2.5}$. These data were corrected for Lorentz-polarization effects, and when two or more peaks overlapped, they were recorded as a single group intensity and similarly treated in any refinement. The Simplex (*5*) method was used to minimize the differences between the observed and calculated intensities. The function minimized was $R = 100 \times \Sigma|I_o - I_c|/\Sigma I_o$. Atomic scattering factors for Ca^{2+}, Mn^{3+} (*6*), and O^{2-} (*7*) were used for the calculations.

For any description of the oxygen-defect nature of $CaMnO_{2.5}$ and $Ca_2MnO_{3.5}$ to be correct, there are several facts that must be

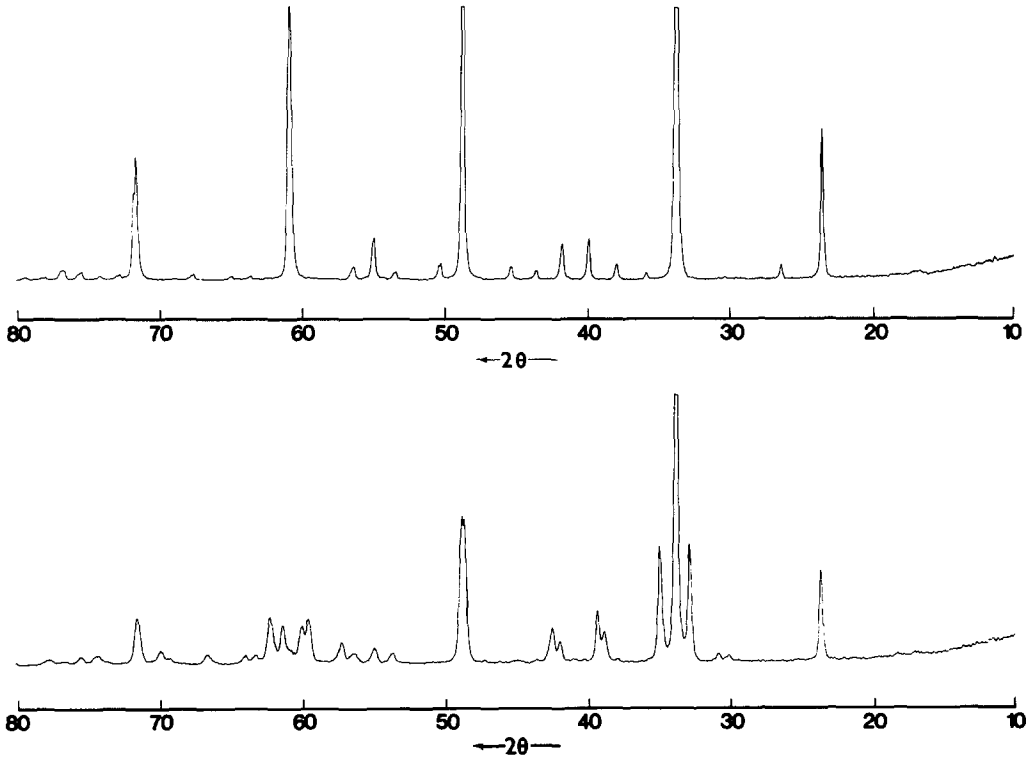

FIG. 3. X-Ray powder diffraction pattern of $CaMnO_{3.0}$ (top) and $CaMnO_{2.5}$ (bottom).

incorporated. First, the similarities in unit cell parameters between perovskite-like $CaMnO_{2.5}$ and K_2NiF_4-like $Ca_2MnO_{3.5}$ imply that the oxygen vacancies order in the sheets of corner-linked $MnO_{4/2}O_{2/2}$ octahedra common to both structures and, more specifically, in the MnO_2 planes and not in the CaO planes. The nearly ideal c dimension of 3.74 Å in $CaMnO_{2.5}$ is consistent with this scheme. Also, the oxygen vacancies must order in the $MnO_{4/2}$ planes in a way to double the shorter pseudotetragonal axis of length $a_c 2^{1/2}$ and be compatible with the electronic configuration of the d^4–Mn^{3+} cations in either a $(t_{2g})^3(d_{z^2})^1$ square pyramidal or $(t_{2g})^3(d_{x^2-y^2})^1$ trigonal bipyramidal configuration. An alternative valence distribution with an equal number of tetrahedral Mn^{2+} and octahedral Mn^{4+} stabilized as in perovskite-related brownmillerite (*8, 9*) is not compatible with these observations.

In oxides with the brownmillerite structure, for example, $CaFeO_{2.5}$ (*9*), the oxygen vacancies are known to order in alternate (001) BX_2 planes of the cubic perovskite, with alternate [110] rows of anions removed (see Fig. 4). This type of vacancy ordering does not double a pseudotetragonal $a_c 2^{1/2}$ axis. If one-half the anions are removed in alternate [110] rows, as shown in Fig. 4, a doubling of an axis occurs and in place of $BX_{4/2}$ sheets of tetrahedral cations, $BX_{5/2}$ sheets of five-coordinate cations with square pyramidal coordination result. These $BX_{5/2}$ sheets are found in $CaMnO_{2.5}$ and $Ca_2MnO_{3.5}$. To maintain the overall composition $CaMnO_{2.5}$ or $Ca_2MnO_{3.5}$, all the perovskite-like $BX_{6/2}$ sheets must contain vacancies. Finally, in $CaMnO_{2.5}$ the vacancies do not appear to order between sheets in a way to give rise to some multiple c dimension. Instead, the equivalent $BX_{3/2}\square_{1/2}X_{2/2}$ sheets appear to be largely controlled by the prismatic coordination around the calcium cations (see discussion).

The ideal atomic positions for $CaMnO_{2.5}$,

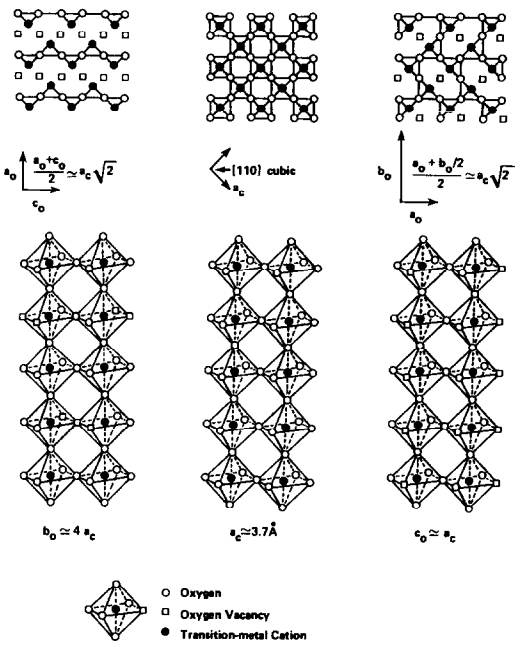

FIG. 4. The structure of stoichiometric ABO_3 perovskite (center), nonstoichiometric $ABO_{2.5}$ brownmillerite (left), and $CaMnO_{2.5}$ (right). The A-cations are not shown.

space group *Pbam*, used as starting positions in the refinement, were: 4 Ca in (h), $x \simeq \frac{1}{4}$, $y \simeq \frac{3}{8}$, $z = \frac{1}{2}$; 4 O(1) in (h), $x \simeq \frac{1}{4}$, $y \simeq \frac{1}{8}$, $z = \frac{1}{2}$ (these are the apical oxygen atoms of the corner-linked $MnO_{4/2}O_{2/2}$ octahedra in $CaMnO_3$ and are in the Ca–O layer with their z coordinate fixed at $\frac{1}{2}$); 4 Mn in (g), $x \simeq \frac{1}{4}$, $y \simeq \frac{1}{8}$, $z = 0$; 4 O(2) in (g), $x \simeq \frac{1}{2}$, $y \simeq \frac{1}{4}$, $z = 0$ (these are the oxygen atoms in the filled $[110]_c$ strings in the $MnO_{1.5}$ layer); and 2 O(3) in (a), $x = 0$, $y = 0$, $z = 0$ (these oxygen atoms are in the half-filled $[110]_c$ strings in the $MnO_{1.5}$ layer). This idealized model gave an agreement factor of $R = 30\%$ based on intensities. Refinement of all position parameters, finally including isotropic temperature factors, resulted in a final $R = 4\%$. The calculated intensities are compared with the observed data for $CaMnO_{2.5}$ in Table I. All refined parameters and some important bond distances and angles are in Table II. Similarly, a reasonable model for

TABLE I

POWDER X-RAY DIFFRACTION DATA FOR $CaMnO_{2.5}$

hkl	d_{calc}[a]	I_{calc}	I_{obsd}	*hkl*	d_{calc}	I_{calc}	I_{obsd}	*hkl*	d_{calc}	I_{calc}	I_{obsd}
020	5.121	0.2	0.4	150	1.917	0.0^+	0.1	251	1.499	0.3	
								161	1.493	17.0	15.0
110	4.799	0.7	0.7	002	1.871	24.5		340	1.478	0.2	
				240	1.863	31.4	55.9	222	1.475	0.1	
001	3.742	4.2	19.0	231	1.848	0.0^+					
120	3.726	16.8						331	1.471	2.6	2.5
				310	1.783	0.3	0.2				
021	3.021	0.1	0.2					142	1.455	2.2	1.7
				022	1.757	0.0^+	0.0				
111	2.951	1.2	1.0					260	1.445	0.2	0.7
				112	1.743	0.1	0.1				
130	2.891	2.1	1.9					170	1.413	0.8	3.9
				320	1.707	2.6		232	1.404	3.1	
200	2.716	25.7	25.5	060	1.707	0.1	3.1				
				151	1.706	0.2		341	1.375	0.1	0.4
121	2.640	93.0	100.0								
210	2.625	6.9		122	1.672	2.0	3.9	400	1.358	1.8	1.7
				241	1.668	1.9		350	1.357	0.2	
040	2.560	28.8	28.8								
				250	1.635	2.4	3.3	261	1.348	0.9	
220	2.399	0.5	0.5	160	1.628	0.9		410	1.346	4.0	5.8
								152	1.339	0.0^+	
140	2.316	6.8	6.7	311	1.610	5.2	5.9				
				330	1.600	0.9		171	1.322	0.0^+	
131	2.288	11.7	12.0					242	1.320	15.3	17.4
				132	1.571	0.2	0.1	420	1.313	0.0^+	
201	2.198	1.4	0.7								
				321	1.553	11.7	11.8				
211	2.149	4.2	4.4	061	1.553	0.5					
230	2.125	8.5	9.6	202	1.541	8.4	10.1				
041	2.113	1.6									
				212	1.524	2.4	3.2				
221	2.020	0.5	0.5								
				042	1.511	10.1	10.7				
141	1.969	0.4	0.2								

[a] Calculated with $a = 5.432$, $b = 10.242$, and $c = 3.742$ Å; $0kl$, $k \neq 2n$, and $h0l$, $h \neq 2n$, are forbidden reflections and were not observed.

$Ca_2MnO_{3.5}$, in space group *Bbam*, would be: 8 Ca in (*i*), $x \simeq \frac{3}{4}$, $y \simeq \frac{1}{8}$, $z \simeq \frac{1}{8}$; 8 O(1) in (*i*), $x \simeq \frac{1}{4}$, $y \simeq \frac{1}{8}$, $z \simeq \frac{1}{8}$; 4 Mn in (*g*) $x \simeq \frac{1}{4}$, $y \simeq \frac{1}{8}$, $z = 0$; 4 O(2) in (*g*), $x \simeq 0$, $y \simeq \frac{1}{4}$, $z = 0$; and 2 O(3) in (*a*), $x = 0$, $y = 0$, $z = 0$. In progress are more accurate structure determinations of $Ca_2MnO_{3.5}$ and $CaMnO_{2.5}$ using powder neutron diffraction data and the technique of profile refinement (*10*).

Evidence for a mixed-valent intermediate phase $CaMnO_{2.75}$ was also observed. Details of its synthesis and characterization will be reported elsewhere (*11*). Preliminary investigations on the intermediate $n = 2$ or 3 members of the series $CaO \cdot nCaMnO_3$, $n = 1, 2, 3$, or ∞, show that they are like Ca_2MnO_4 ($n = 1$) and $CaMnO_3$ ($n = \infty$) in their oxygen deficiency.

TABLE II

ATOM PARAMETERS, BOND DISTANCES, AND ANGLES FOR $CaMnO_{2.5}$

Atom	Site	x	y	z	B (Å)^2
Ca	$4h$	0.3039(5)[a]	0.3636(5)	½	0.2(1)
O(1)	$4h$	0.2971(10)	0.0985(10)	½	1.2(1)
Mn	$4g$	0.2773(5)	0.1173(5)	0	1.0(1)
O(2)	$4g$	0.047(10)	0.281(10)	0	2.4(5)
O(3)	$2a$	0	0	0	1.0(1)

Selected bond distances (Å) and angles (°)

Mn	–O(1)	1.883(5)[b]	[2x][c]	Ca	–O(2)	2.482(47)	[2x]
Mn	–O(2)	2.093(88)	[1x]	Ca	–O($2a$)	2.727(62)	[2x]
Mn	–O($2a$)	1.796(74)	[1x]	Ca	–O($3a$)	2.565(5)	[2x]
Mn	–O(3)	1.927(4)	[1x]	Ca	–O(1)	2.714(12)	[1x]
				Ca	–O($1a$)	2.708(8)	[1x]
O(3)	–Mn–O(2)	91.8(2)		Ca	–O($1b$)	2.466(11)	[1x]
O(3)	–Mn–O(1)	88.9(3)		Ca	–O($1c$)	2.781(8)	[1x]
O(2)	–Mn–O($2a$)	91.4(4)					
O(2)	–Mn–O(1)	96.7(3)		Mn(1)	–Mn($1a$)	3.409(7)	
O($2a$)	–Mn–O(1)	90.7(4)		O($1b$)	–O($1c$)	2.988(12)	

[a] The errors (in parentheses) are estimated from a series of determinations.
[b] The errors in bond distances and angles refer to one standard deviation.
[c] Frequency of occurrence as nearest neighbors of the cation.

Discussion

The differences between structures of oxygen-deficient compounds of the type ABO_{3-x}, where A is an alkaline earth cation and B is a transition metal ion, are a direct consequence of preferred coordination schemes for the reduced ions, and manganese is not an exception. The defect structure of $CaMnO_{2.5}$ is shown in detail in Fig. 5. Since the K_2NiF_4 structure type (*12*) contains identical perovskite sections, the defect nature of $Ca_2MnO_{3.5}$ is analogous to that represented in Fig. 5 and will not be discussed here in any detail. The structure of $CaMnO_{2.5}$ is characterized by oxygen vacancies generated by the reduction of Mn^{4+} to Mn^{3+}. These vacancies order in the (001) plane with alternate [100] strings of oxygen atoms (on orthorhombic basis) missing every other oxygen. The vacancies are displaced by $a_o/2$ in alternate strings. Thus the manganese ions are coordinated by five oxygen ions as opposed to octahedral coordination in the oxidized form. The coordination around the Mn^{3+} cations approximates square pyramidal with O–Mn–O bond angles ranging from 89 to 97° in $CaMnO_{2.5}$. The additional electron of high-spin Mn^{3+} occupies the d_{z^2} orbital with the $d_{x^2-y^2}$ orbital on the metal used in Mn–O σ bonds and $sp^3d_{x^2-y^2}$ states characteristic of square pyramidal geometry. The unequal occupation of the d_{z^2} and $d_{x^2-y^2}$ orbitals results in a long Mn–O(2) distance of 2.09 Å that is trans to the oxygen vacancy. This results in O($2a$) being strongly π donating to Mn(1) and is reflected in the short 1.80 Å bond distance between Mn(1) and O($2a$). Other Mn–O bond distances of 1.88 Å to O(1) and 1.93 Å to O(3) reflect the range in metal–oxygen distances that are characteristic of the oxidized precursor. In this simple, yet elegant, fashion the lattice has synergistically stabilized around each manganese site the differentiating electron, an oxygen va-

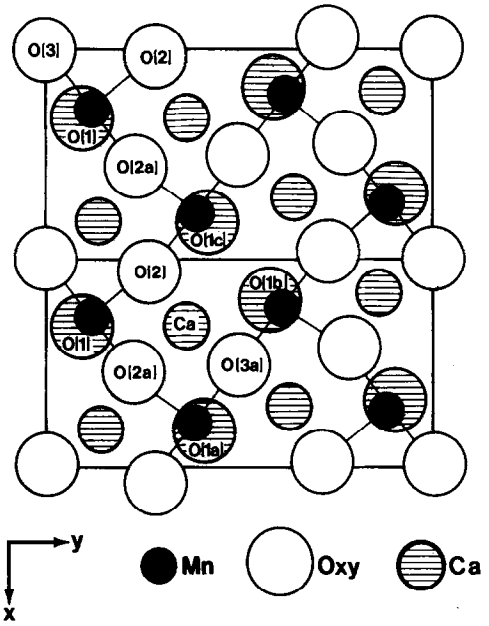

FIG. 5. The projection down the c axis of the structure of $CaMnO_{2.5}$. Atoms are at $z = 0$ (open and solid circles) or $z = \frac{1}{2}$ (hatched circles).

cancy, and the induced π character of O(2). The only other example of an oxide with Mn^{3+} having approximately the same coordination as $CaMnO_{2.5}$ is the compound $Na_2MnO_{2.5}$ (*13*). In this compound, the low-field sodium cation occupies an octahedral site and Mn^{3+} is five-coordinate in an ordered oxygen vacancy derivative of the sodium chloride structure.

A reasonable modification of our structural model for $CaMnO_{2.5}$ would be a doubling of the 3.7-Å c axis to reflect a $b_0/2$ shift in the position of the oxygen vacancy in alternate $MnO_{1.5}$ planes. No evidence could be found for this additional type of order in the powder data. The reason for this result appears to be the coordination requirements of the calcium ions. As can be seen in Fig. 5, the coordination around the calcium cation is approximately that of a tricapped trigonal prism with an additional more distant oxygen. The regular (4 + 4 + 4) coordination around the A cation in perovskite has changed to (3 + 4 + 3) due to the oxygen vacancies in the (001) plane. Two of the three prism faces remain capped much as they were in the oxidized form, and the third face of the prism clearly attracts O(1b) (2.47 Å) more strongly than O(1c) (2.78 Å). This translational pinning of the oxygen vacancies in continuous strings along [001] may account, on the microscopic level, for the low activation barriers to reduction and oxidation of these materials.

The infrared spectra of $CaMnO_3$ and $CaMnO_{2.5}$ are compared in Fig. 2. Identical spectra can be obtained after any number of reduction cycles followed by reoxidation. These data, like the X-ray and TGA results, are consistent with a reversible reaction. Some of the metal–oxygen stretching modes in the region 600–800 cm^{-1} are shifted to higher frequency in $CaMnO_{2.5}$. The positions of these bands in the infrared are characteristic of the π character of the bond between Mn(1) and O(2a).

In combination with MnO_2, the more basic alkaline earth oxides SrO and BaO form a variety of structures based on mixed hexagonal and cubic close-packed BaO_3 layers. Negas and Roth (*14, 15*) have extensively studied the $SrMnO_{3-x}$ and $BaMnO_{3-x}$ systems and have concluded that transformations between structures are not truly polymorphic, but rather are associated with their oxygen content. The nonstoichiometry was rationalized in terms of oxygen vacancies in either cubic or hexagonal close-packed AO_3 layers. In their proposed model, an anion vacancy in a cubic layer would result in two nonbridging Mn^{3+} five-coordinative groups, as opposed to two five-coordinate Mn^{3+} ions sharing an edge if the anion vacancy occurred in a hexagonal layer. Small cation and anion displacements were assumed to occur such that either site would distort to a more or less regular trigonal bipyramidal geometry, rather than remain square pyramidal. $YMnO_3$ (*16*) was

cited as an example of Mn^{3+} with trigonal bipyramidal coordination by oxygen. On the basis of compositional and X-ray data, Negas and Roth recognized that stabilization of cubic stacking was related to the reduction process in both $SrMnO_{3-x}$ and $BaMnO_{3-x}$ and concluded that the long face-sharing sequences in the 2L, 15L, and 8L structures could not tolerate large Mn^{3+} concentrations. In the 6L and 10L forms, they recognized that the limiting stoichiometries were near $Ba_6Mn_4^{4+}Mn_2^{3+}O_{17}$ and $Ba_{10}Mn_6^{4+}Mn_4^{3+}O_{28}$, which they correlated with the number of Mn^{3+} cations and an equivalent number of manganese positions in double face-shared units. In addition, this model permitted all Mn^{4+} cations to order in the long face-sharing sequences. Their conclusion that the oxygen vacancies were localized in the AO_3 layers of hexagonal symmetry, but *only* between the face-shared pairs of manganese cations, results in layers with the composition AO_2 and edge-shared pairs of Mn^{3+} cations. In a powder neutron diffraction investigation of the oxygen vacancy distribution in 4L–$Ba_{0.5}Sr_{0.5}MnO_{2.84}$ Jacobson and Horrox (*17*) concluded that the oxygen vacancies were, indeed, distributed in hexagonal layers (face-shared positions) and that oxygen sites in cubic layers (corner-linked octahedra) were fully occupied. No evidence for vacancy ordering could be detected with the powder neutron diffraction data, or by electron microscopy on an annealed sample. The nature of the powder X-ray diffraction patterns of samples quenched from high temperature did not allow Negas and Roth (*14, 15*) to detect incipient vacancy ordering in their materials.

The preparation of $CaMnO_{2.5}$ by the low-temperature reduction of crystalline $CaMnO_3$ resulted in powder diffraction patterns with sufficient detail that a determination of the vacancy ordering in $CaMnO_{3-x}$ was possible. This description, based on a network of CaO and $MnO_{1.5}$ layers derived from cubic perovskite, made the comparison of $CaMnO_{2.5}$ with $CaFeO_{2.5}$ (brownmillerite) possible. In order to compare structures with hexagonal AO_3 layers mixed with cubic layers, it is necessary to focus on close-packed AO_3 layers with either hexagonal (h) or a cubic (c) symmetry, and to view the B cations as occupying the octahedral interstices formed between layers. Applying this alternative description to $CaMnO_{2.5}$, we find that the anion vacancies occur in all layers to the same extent. That is, each layer has a composition $CaO_{2.5}$ and square pyramidal (C_{4v}) coordination is maintained around the Mn^{3+} cations. We propose for the composition-dependent polytypes in the series $SrMnO_{3-x}$ and $BaMnO_{3-x}$ that the vacancies do not concentrate in AO_2 layers of either cubic or hexagonal symmetry, but instead form $AO_{2.5}$ planes in layers of only cubic close-packing symmetry. Whereas Negas and Roth (*15*) suggested that the stabilization of cubic stacking upon reduction was a direct result of the tolerance by the structure of a greater concentration of Mn^{3+} ions of larger radii, we suggest that the cubic layers result from the introduction of manganese–oxygen vacancy pairs. For example, 6L–$BaMnO_{2.83}$ and 10L–$BaMnO_{2.80}$ would have the correct stoichiometry with two and four $BaO_{2.5}$ layers, respectively.

Conclusions

The oxygen-deficient compounds $CaMnO_{2.5}$ and $Ca_2MnO_{3.5}$ are examples of new compounds that can be prepared as a result of the preservation of essential structural features that exist in the starting materials. These materials are notable in that reoxidation, which occurs at an appreciable rate at 300°C, restores their initial composition and structure. Finally, we have shown that the distribution of oxygen vacancies in $CaMnO_{2.5}$ and $Ca_2MnO_{3.5}$ is a consequence of the square pyramidal coordination of Mn^{3+}, al-

though trigonal bipyramidal coordination with Mn^{3+} covalently bonded to two axial oxygen atoms might have been expected.

Acknowledgments

The authors express their thanks to Mr. J. Dunn for the preparation of the materials used in this work. We also thank Mr. H. Brady for the powder X-ray diffraction data, Dr. J. Brown for the FTIR spectra, and Professor A. Wold of Brown University for the susceptibility measurements.

References

1. J. B. GOODENOUGH AND J. M. LONGO, Landolt-Bornstein, Group III/Vol. 4a, Springer-Verlag, New York/Berlin (1970).
2. H. S. HOROWITZ AND J. M. LONGO, *Mater. Res. Bull.* **13,** 1359 (1978).
3. J. B. MACCHESNEY, H. J. WILLIAM, J. F. POTTER, AND R. C. SHERWOOD, *Phys. Rev.* **164,** 779 (1967).
4. S. H. RUDDLEDEN AND D. POPPER, *Acta Crystallogr.* **10,** 538 (1957).
5. J. A. NELDER AND R. MEAD, *Comput. J.* **7,** 308 (1965).
6. D. T. CROMER AND J. T. WABER, *Acta Crystallogr.* **18,** 104 (1965).
7. M. TOKONAMI, *Acta Crystallogr.* **19,** 486 (1965).
8. W. C. HANSEN AND L. T. BROWNMILLER, *Amer. J. Sci.* **15,** 224 (1928).
9. E. F. BERTAUT, P. BLUM, AND A. SAGNIERES, *Acta Crystallogr.* **12,** 149 (1959).
10. H. M. RIETVELD, *Acta Crystallogr.* **22,** 151 (1967).
11. R. A. BEYERLEIN, private communication.
12. A. F. WELLS, "Structural Inorganic Chemistry," 4th ed., p. 498, Oxford Univ. Press (Claredon), Oxford (1975).
13. G. BRACHTEL AND R. HOPPE, *Z. Anorg. Allg. Chem.* **468,** 130 (1980).
14. T. NEGAS AND R. S. ROTH, *J. Solid State Chem.* **1,** 409 (1970).
15. T. NEGAS AND R. S. ROTH, *J. Solid State Chem.* **3,** 323 (1971).
16. H. YAKEL, W. C. KOEHLER, E. F. BERTAUT, AND F. FORRAT, *Acta Crystallogr.* **16,** 957 (1963).
17. A. J. JACOBSON AND A. J. W. HORROX, *Acta Crystallogr. Sect. B* **32,** 1003 (1976).